

Computational Aeroelastic Analysis of the Semi-Span Super-Sonic Transport (S⁴T) Wind-Tunnel Model

Mark D. Sanetrik* and Walter A. Silva†

Aeroelasticity Branch, NASA Langley Research Center, Hampton VA, 23681

Jiyoung Hur‡

Lockheed Martin, NASA Langley Research Center, Hampton, VA 23681

A summary of the computational aeroelastic analysis for the Semi-Span Super-Sonic Transport (S⁴T) wind-tunnel model is presented. A broad range of analysis techniques, including linear, nonlinear and Reduced Order Models (ROMs) were employed in support of a series of aeroelastic (AE) and aeroservoelastic (ASE) wind-tunnel tests conducted in the Transonic Dynamics Tunnel (TDT) at NASA Langley Research Center. This research was performed in support of the ASE element in the Supersonics Program, part of NASA's Fundamental Aeronautics Program. The analysis concentrated on open-loop flutter predictions, which were in good agreement with experimental results. This paper is one in a series that comprise a special S⁴T technical session, which summarizes the S⁴T project.

I. Introduction

The unique design elements required for efficient supersonic flight, such as a long, narrow fuselage and thin wings with sharp leading edges, can result in highly complex nonlinear aeroelastic and flight dynamics phenomena. The Semi-Span, Super-Sonic Transport (S⁴T) project was designed to investigate this problem. This paper is part of a special session covering the computational and experimental research conducted on the S⁴T wind-tunnel model. It presents an overview of the linear and nonlinear computational analyses performed during the project. The S⁴T project was conducted by the Aeroelasticity Branch at the NASA Langley Research Center under the auspices of the Supersonics Project of the NASA Fundamental Aerodynamics Program (FAP). Further detail of the S⁴T project and the FAP can be found in other papers to be presented as part of this special session^{1,2}. The purpose of the wind-tunnel tests, conducted at NASA Langley's Transonic Dynamics Tunnel (TDT), was to supply data to design and test control laws designed to improve ride quality, alleviate gust loads and suppress flutter. The wind-tunnel test program consisted of four entries into the TDT. The first two test, both open-loop (control law off), were used to obtain system identification data, which was used to build Linear Time Invariant (LTI) state-space models of the system. These state-space models were used to design the control laws, which were tested and evaluated in the final two tests, both closed-loop (control law on). The computational effort has concentrated on open-loop flutter calculations, as well as basic aerodynamic analysis of the S⁴T configuration.

The paper begins with a brief description of the Finite Element Model (FEM) that was used throughout the analysis process. It continues with a description of the linear analysis using MSC Nastran®, and the inviscid and viscous nonlinear analysis using the aeroelastic version of the block-structured Computational Fluid Dynamics (CFD) code CFL3D Version 6.4³. Next, results are shown for the additional analysis of the S⁴T configuration using Reduced Order Models (ROMs), which were created using the computational solutions from CFL3D. Finally, a summary of the results and a discussion of future work are presented.

* Aerospace Engineer, Aeroelasticity Branch, Senior Member, AIAA.

† Senior Research Scientist, Aeroelasticity Branch Associate Fellow, AIAA.

‡ Senior Aeronautical Engineer, Lockheed Martin Mission Services.

II. Modal Analysis

As part of the design process, a detailed Finite Element Model (FEM) of the S⁴T wind-tunnel model was developed. The FEM consists of 2866 points and 4530 elements. Figure 1 shows a view of the FEM; a complete description of the development of the FEM can be found in another paper to be presented as part of this special session². This FEM was the basis of the modal and flutter analyses conducted using MSC Nastran. The FEM was updated throughout the course of the project as more was learned about the structural characteristics of the actual wind-tunnel model. One of the most important indications of the accuracy of the FEM is a comparison of the structural mode shapes and frequencies obtained by the Nastran modal analysis with the results obtained from Ground Vibration Tests (GVTs) of the actual wind-tunnel model. Table 1 shows a comparison of the frequencies of the first four flexible modes between the Nastran analysis and a typical GVT result. Note that the frequencies compare well except for mode 2, which has a difference of approximately 7%. Multiple GVTs were performed during the course of the project; the resulting frequencies varied from test to test, with no test exactly agreeing with the Nastran analysis. Figure 2 shows the first flexible mode shape from the Nastran analysis, while Fig. 3 shows the first mode shape from the GVT. The second, third, and fourth flexible mode shapes from the Nastran analysis are shown in Fig. 4, 6 and 8 respectively, while Fig. 5, 7, and 9 show the corresponding mode shapes from the GVT. The mode shapes from the Nastran analysis agree well with the mode shapes obtained from the GVT analysis. Additional detail for the GVT procedure can be found on another paper to be presented as part of this special session².

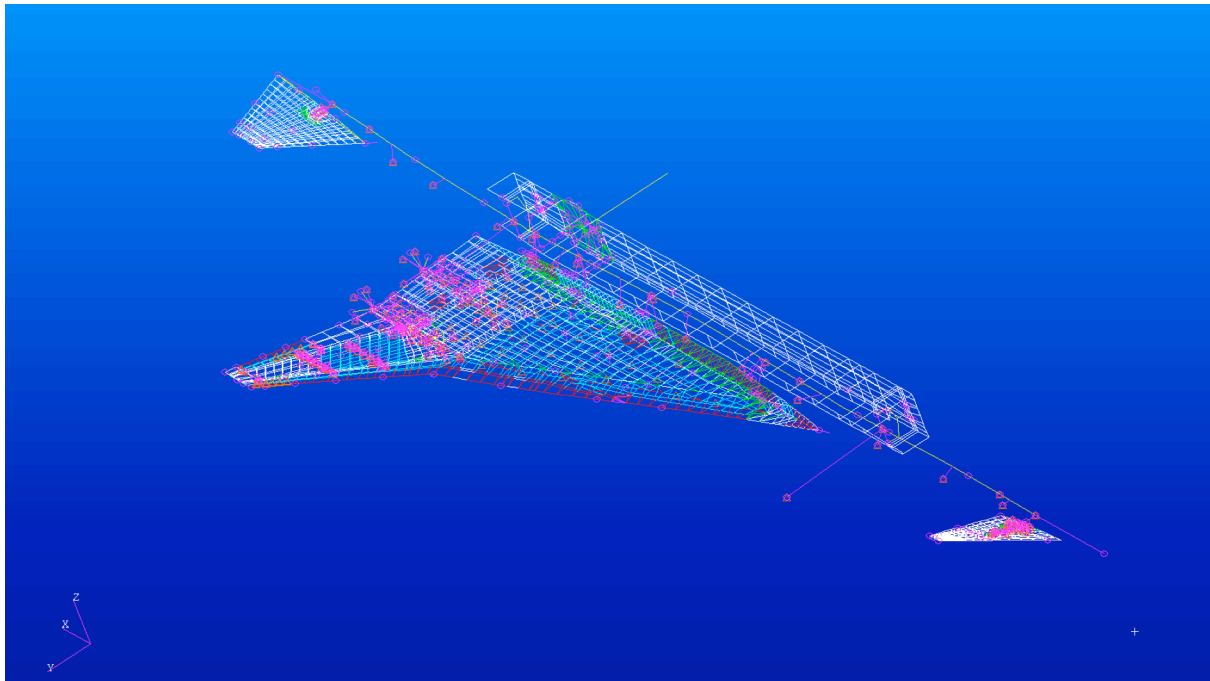


Figure 1. Finite Element Model

Mode	Mode Description	Nastran Frequency (Hz)	GVT Frequency (Hz)	Percent Difference
1	Pitch about forward nodal mount	6.290	6.249	0.65
2	Pitch about balance	8.435	7.838	7.34
3	Fuselage bending	10.074	10.059	0.15
4	Wing bending	11.401	11.781	3.28

Table 1. Comparison of modal frequencies between the Nastran analysis and GVT.

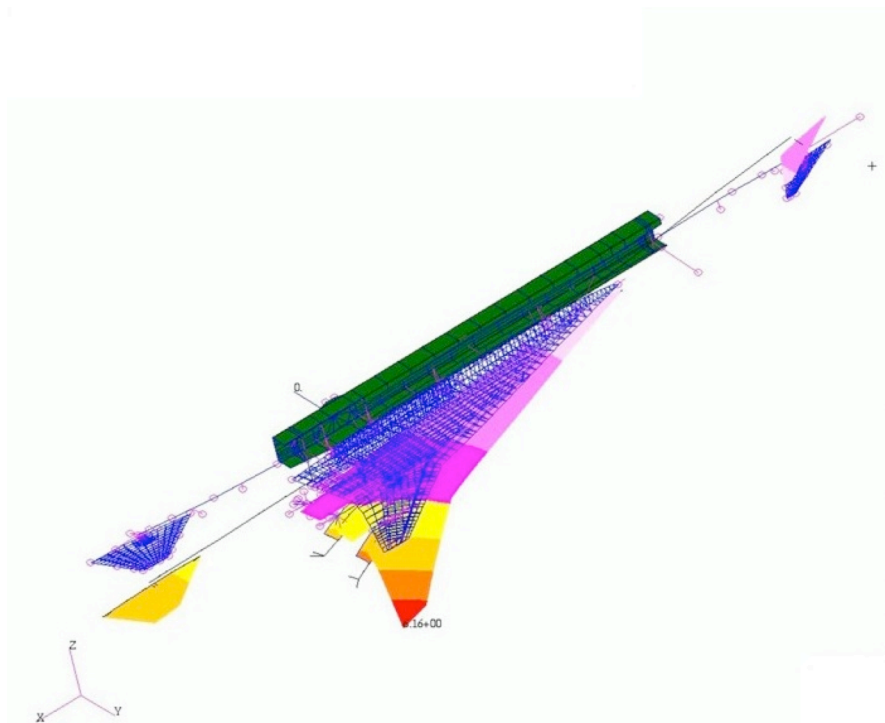


Figure 2. First flexible mode from finite element analysis.

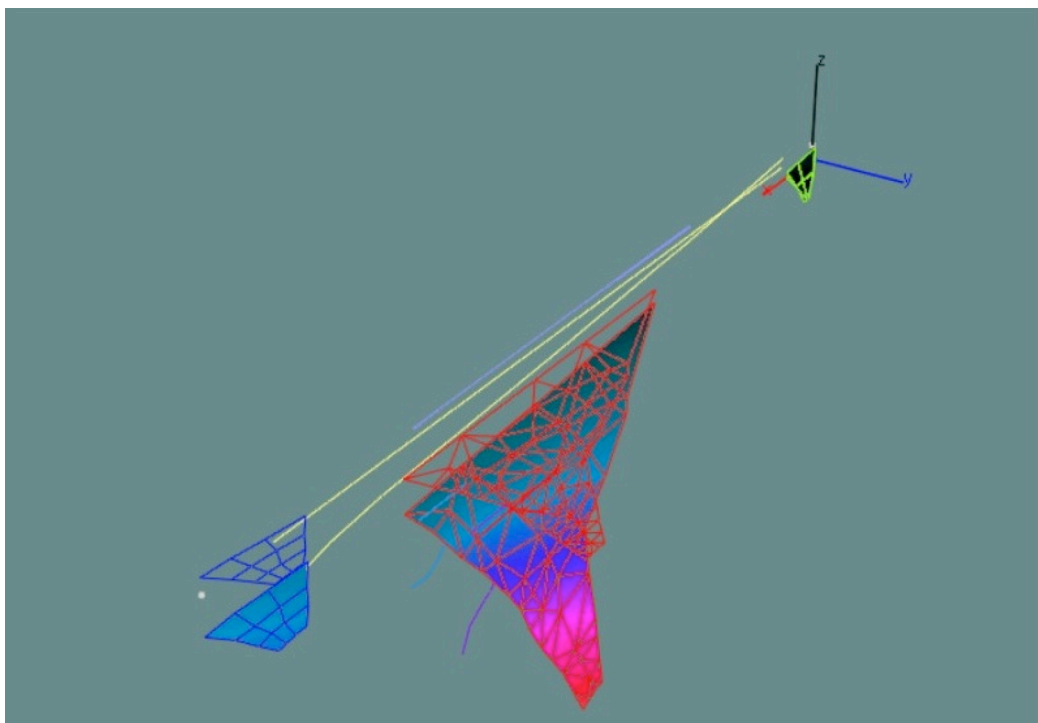


Figure 3. First flexible mode from GVT.

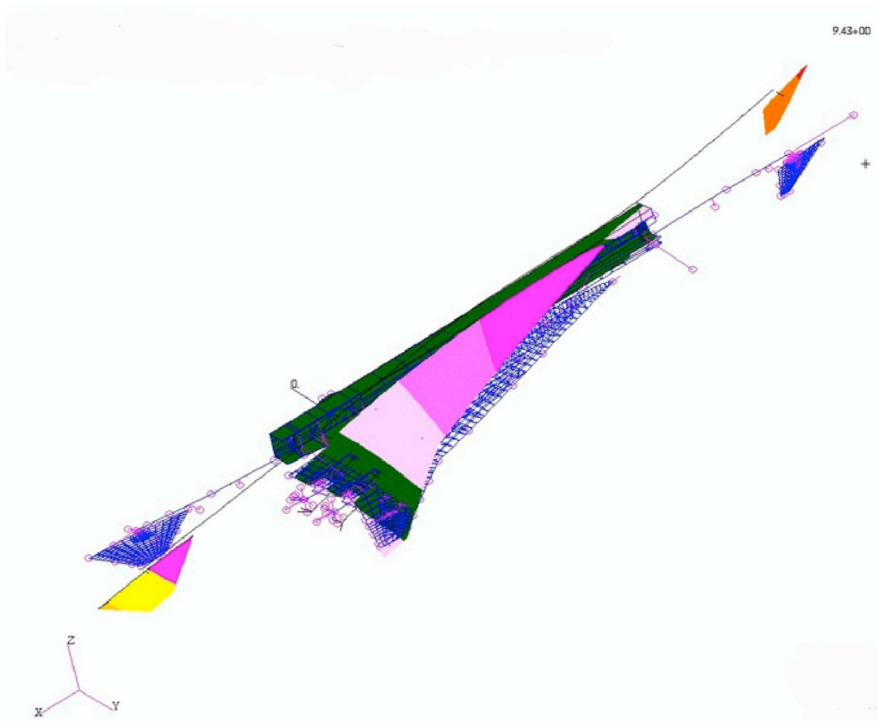


Figure 4. Second flexible mode from finite element analysis.

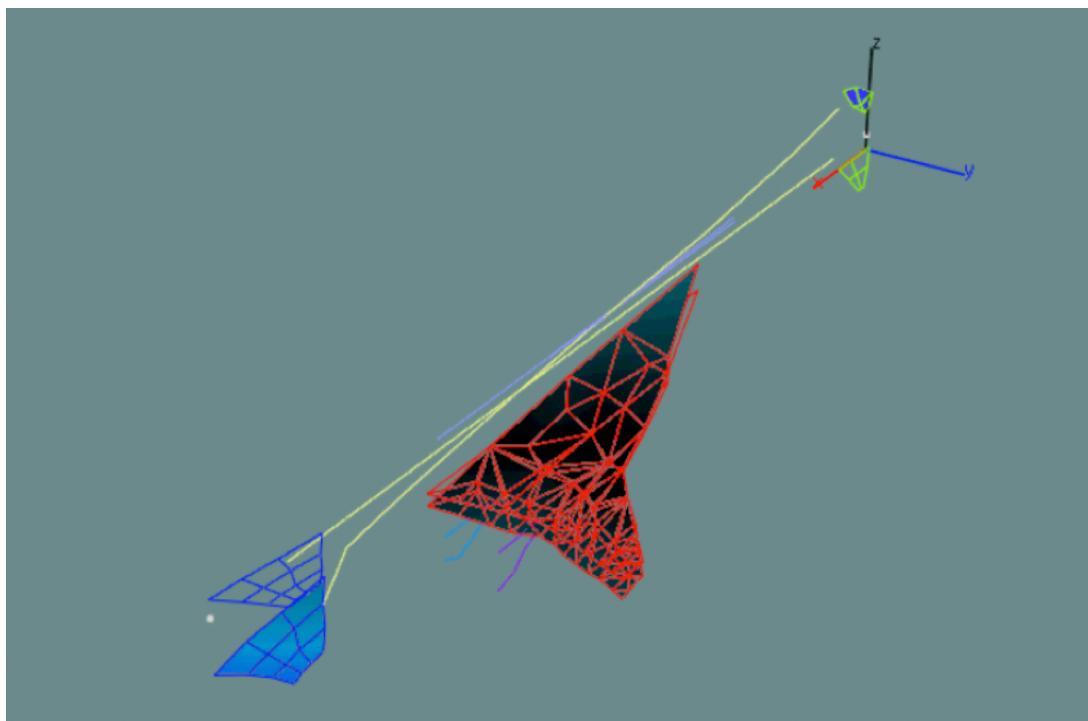


Figure 5. Second flexible mode from GVT.

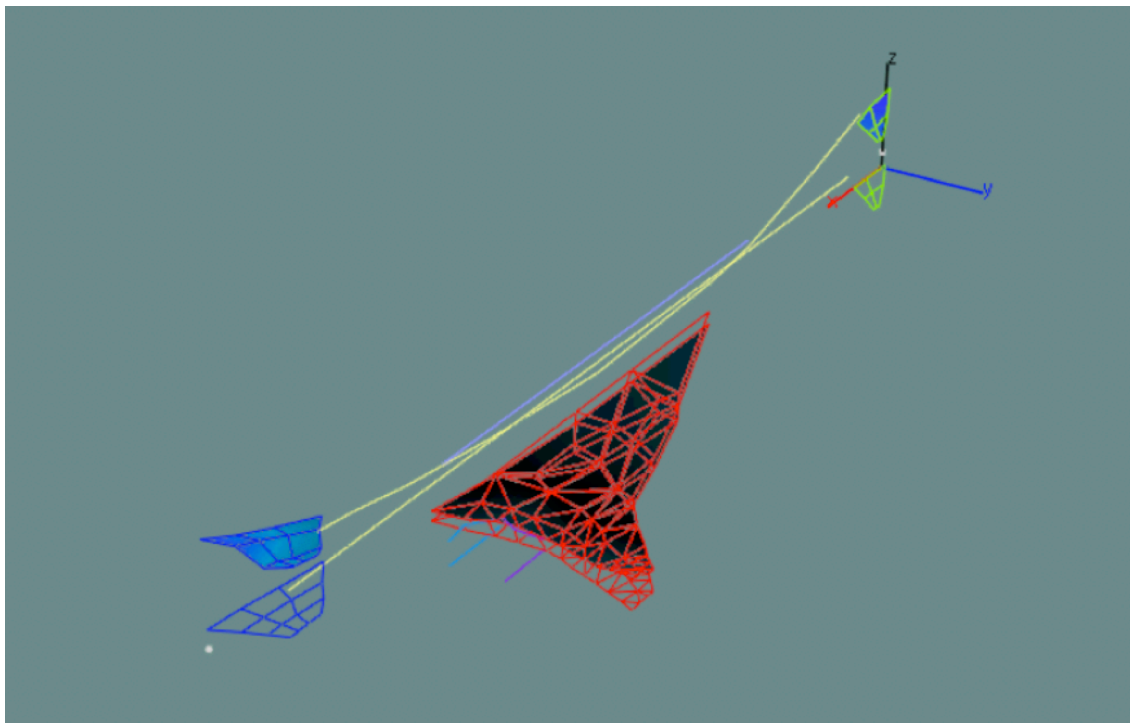
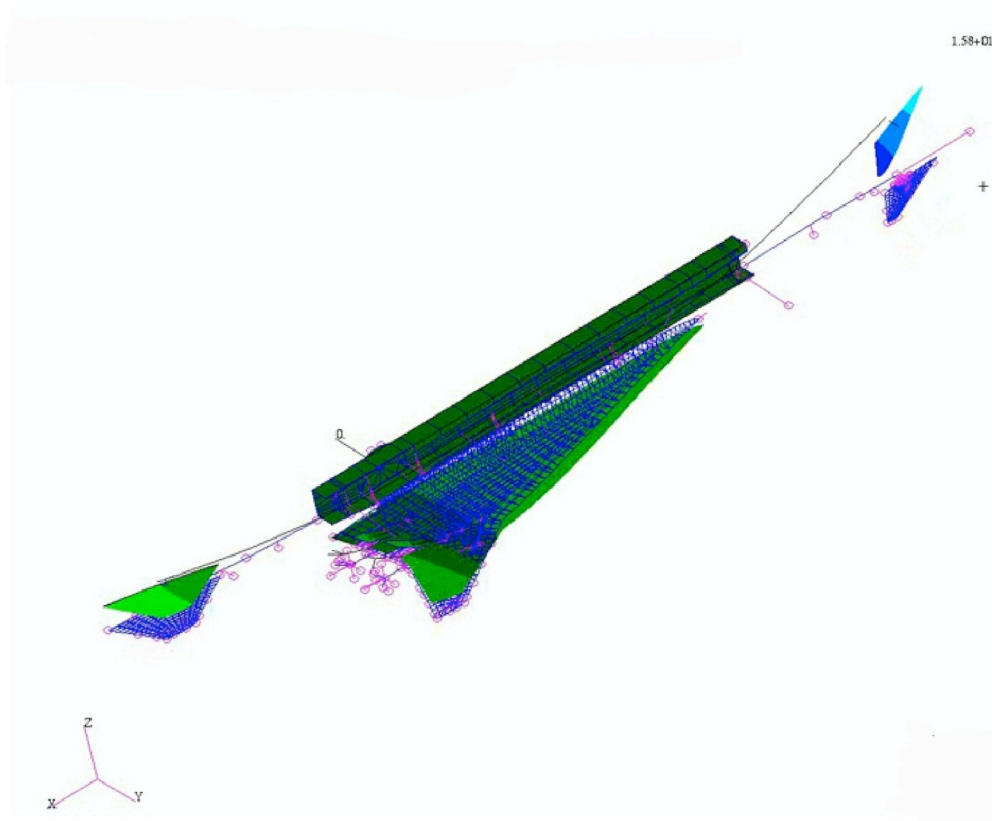


Figure 7. Third flexible mode from GVT.

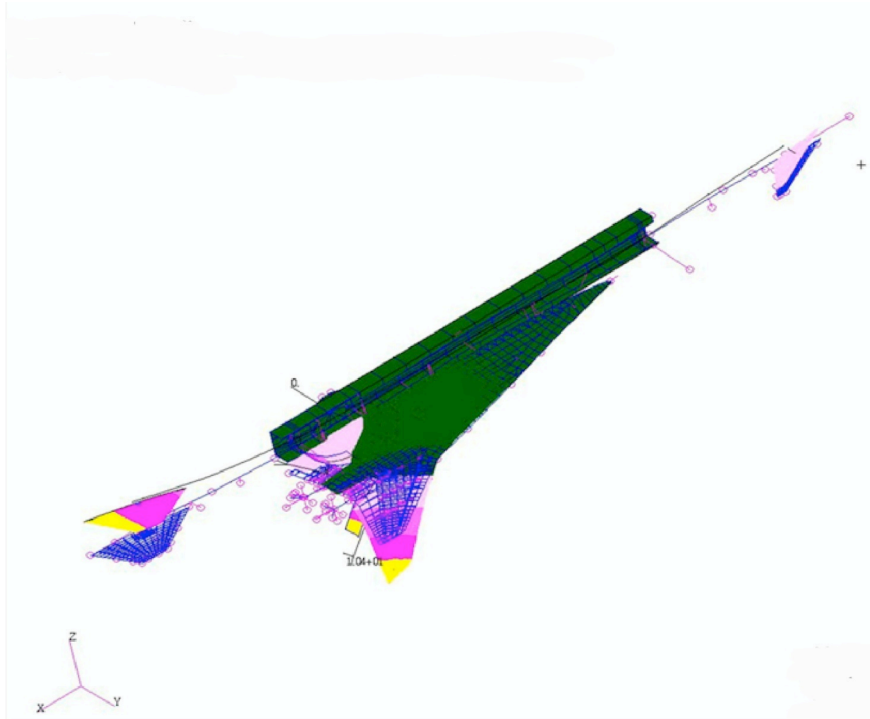


Figure 8. Fourth flexible mode from finite element analysis.

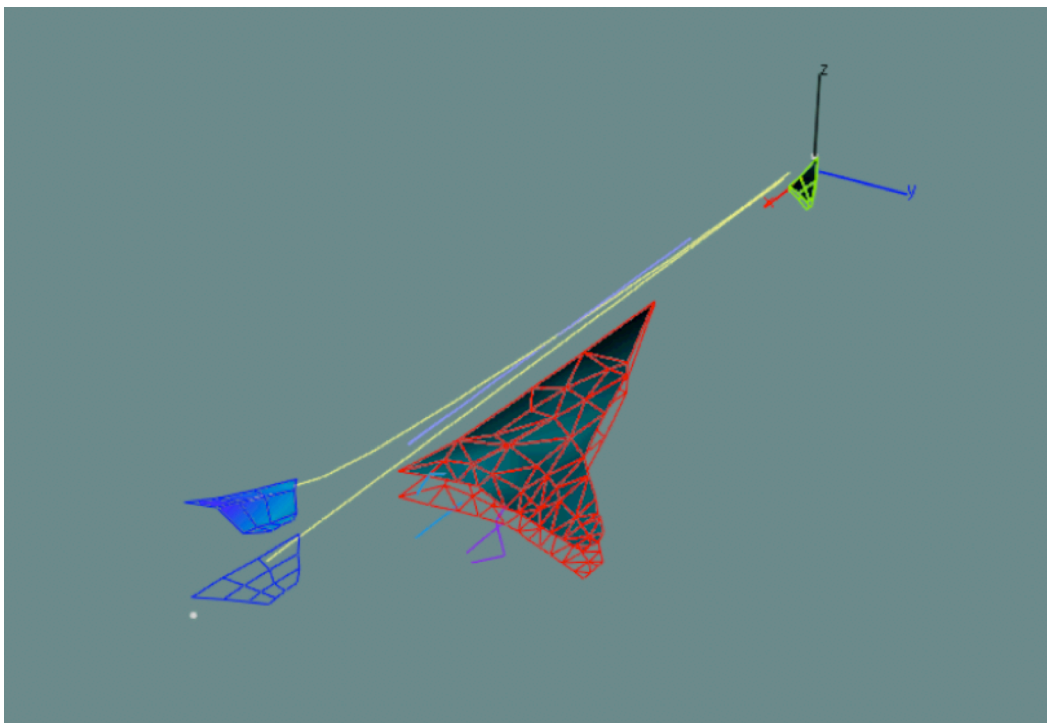


Figure 9. Fourth flexible mode from GVT.

The flexible modes that were obtained from the Nastran analysis were also an important part of the Computational Aeroelastic (CAE) analysis. The first step in the CAE analysis procedure was to interpolate the flexible modes from the Nastran analysis onto the CFD surface grid. This is a complex process even for simple configurations. The unique design of the S⁴T wind-tunnel model made the interpolation processes even more challenging. The main structural element of the wind-tunnel model is a flexible composite fuselage beam, to which is attached the Ride Control Vane (RCV), wing and horizontal tail. Covering this flexible beam was a rigid fiberglass fuselage shell that was attached directly to the backstop. Slots were cut in the fuselage shell to allow for the vertical movement of the RCV and horizontal tail due to the deflection of the flexible beam, while a gap between the wing and fuselage shell allowed for the vertical movement of the wing. Transferring the mode shapes for the flexible beam to the computational fuselage surface would imply that the fuselage shell was free to deflect, which was not the case. A special procedure was developed that zeroed out the mode shapes on the majority of the fuselage and smoothly blended them in the vicinity of the RCV, wing, and horizontal tail. The process began by transferring the mode shapes to the computational surface grid, but only for the RCV, wing, horizontal tail, and a small section of the fuselage adjacent to these surfaces. The results from this procedure for the second flexible mode can be seen in Fig. 10, while Fig. 11 shows a detailed view of the region around the RCV, showing essentially constant deflection for the RCV and the patch of fuselage. Having the deflections change discontinuously to zero at the edges of the fuselage patches could cause problems for the grid deformation procedure used in CLF3D. A procedure was developed to smoothly blend the deflection to zero at the edges of the fuselage patches. Figure 12 shows the results of this procedure applied to the region near the RCV, displayed as contour lines with the grid lines shown. The deflection for the RCV has remained at its original value of 1.0. However, the smooth concentric contour lines on the fuselage patch show the deflection transitioning from a value of 1.0 at the RCV root to a value of 0.0 at the outer edge of the patch. Figure 13 shows the same results in terms of smoothly shaded contours. Figure 14 shows the vertical deflection of the RCV, wing and horizontal tail due to the second flexible mode after the procedure has been fully implemented.

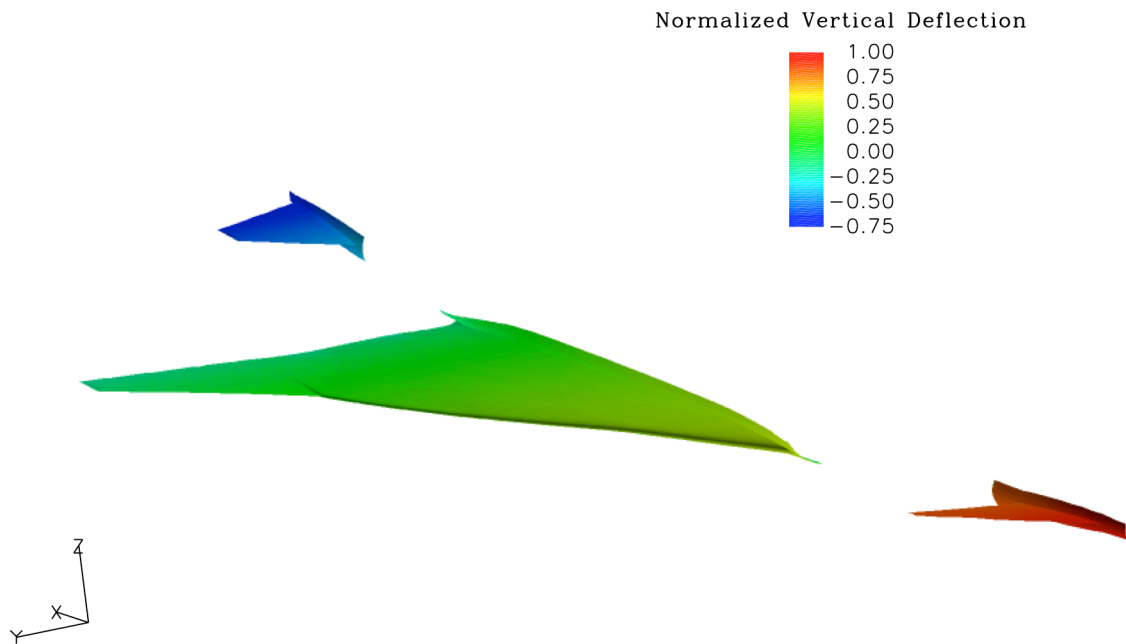


Figure 10. Vertical deflection for flexible mode 2 interpolated onto portions of the computational surface grid.

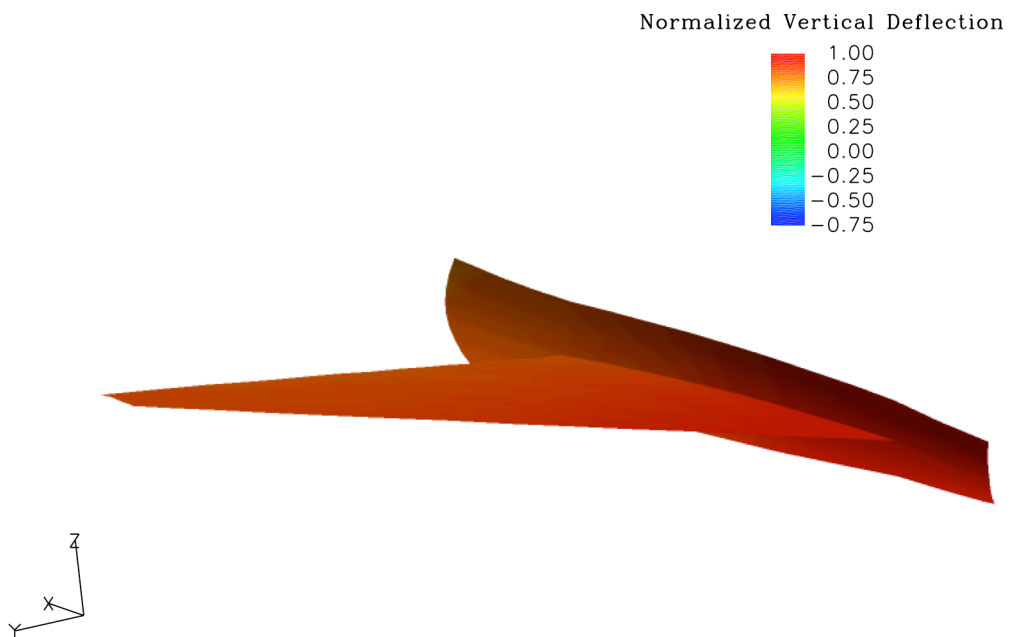


Figure 11. Detail of deflection near the RCV.

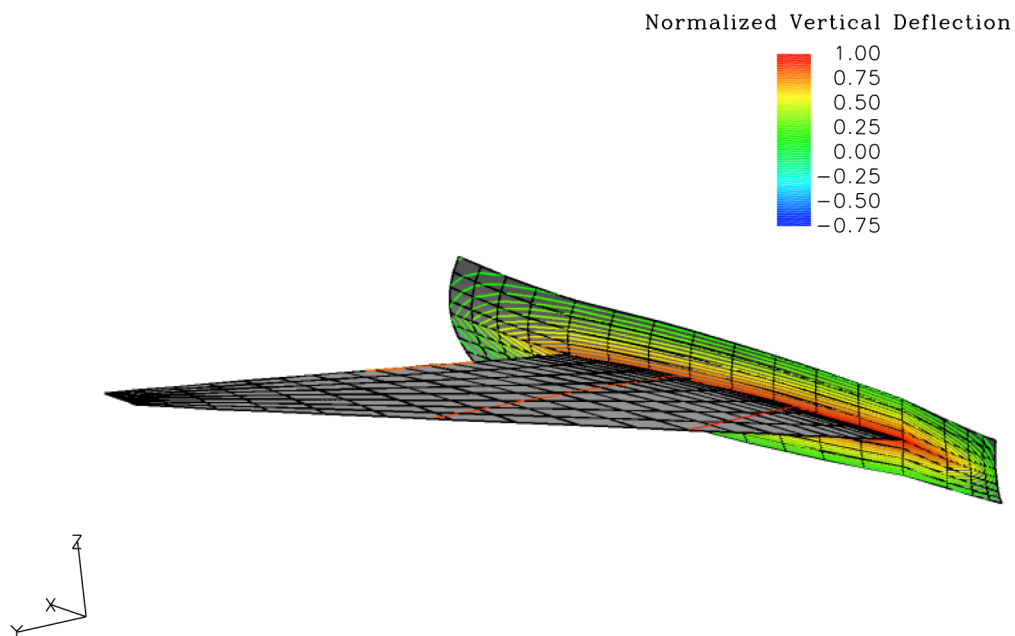


Figure 12. Smoothed deflections near the RCV shown as contour lines.

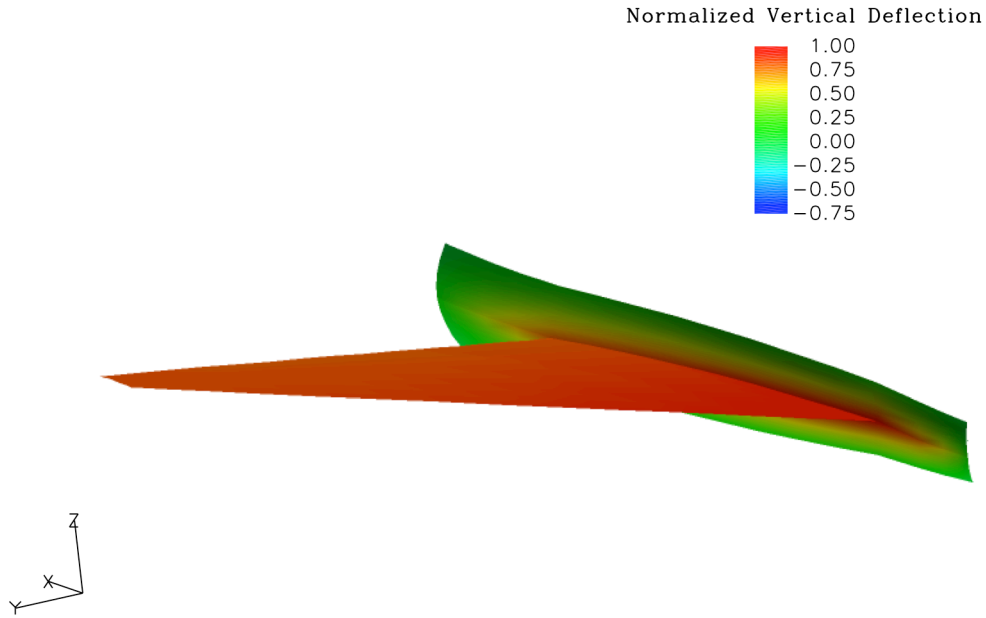


Figure 13. Smoothed of deflections near the RCV shown as smooth shading.

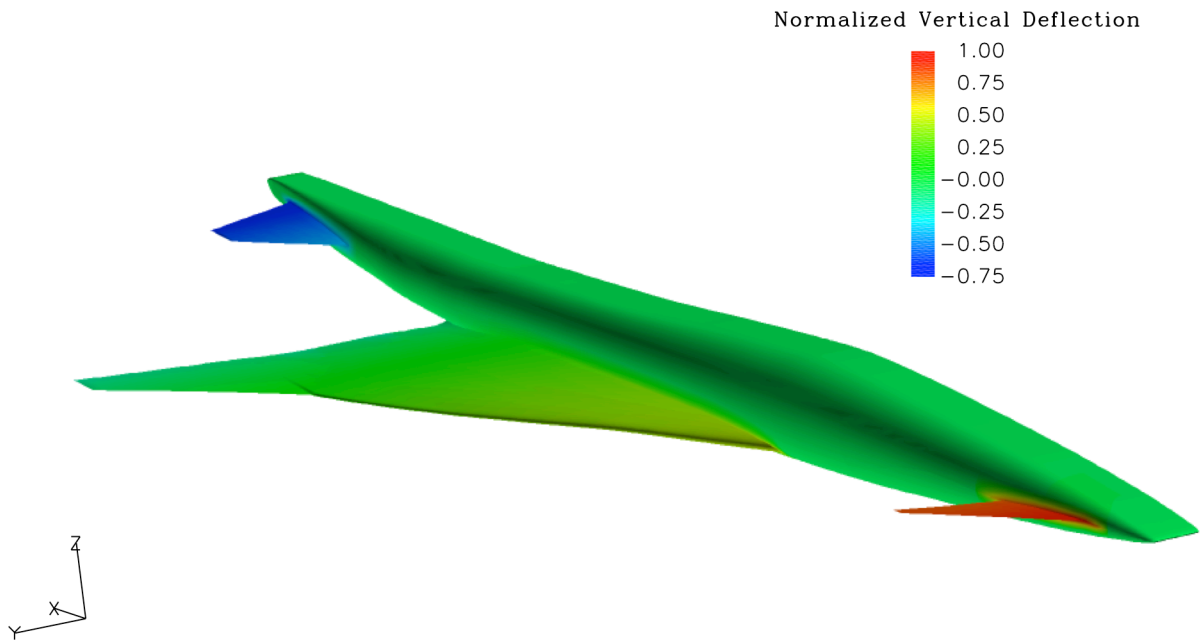


Figure 14. Final deflections for flexible mode 2 interpolated the computational surface grid.

III. Linear Aeroelastic Analysis

Linear analysis was used extensively throughout the test program. MSC Nastran® was used for this analysis; the doublet lattice method was used to calculate subsonic aerodynamics and the ZONA51 method was used for supersonic flow. The first thirty flexible modes (up to a frequency of 97 Hz) were used in the flutter analysis. For each analysis, the velocity was held constant, while the density was increased such that the dynamic pressure increased from 10 psf to 500 psf in increments of 10 psf. This mimicked the procedure used during the wind-tunnel tests. Figure 15 shows the doublet lattice aerodynamic box layout used in the linear analysis. The faster turn-around time for linear solutions compared to nonlinear computations made the linear analysis ideal for quickly determining the effect of changes made to the FEM. One of the features of the S⁴T wind-tunnel model was the ability to change the dynamics of the configuration by adjusting the weight of the engine nacelles and the stiffness of the pylons attaching the engines to the wing. Two pylons were available: one with nominal stiffness, and a second with 75% of nominal stiffness. Tungsten rods could also be added to the periphery of each nacelle; the rods were available to increase the weight of the nacelles by a factor of 1.5, 2.0, and 2.5 times the nominal (empty) nacelle weight. A full description of the wind-tunnel model can be found in another paper that has been submitted as part of the S⁴T special session¹.

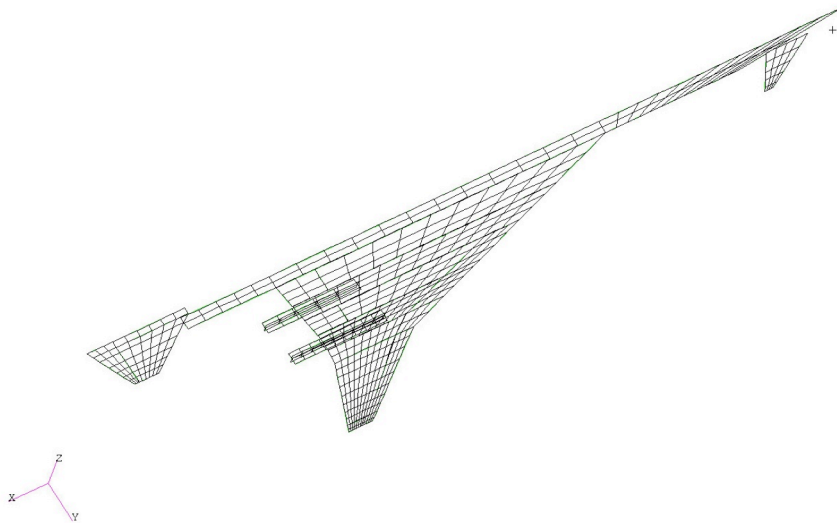


Figure 15. Doublet lattice box layout used in the linear analysis.

Before the first open-loop test, a parametric study was conducted to determine the effect of engine weight and pylon stiffness on the flutter boundary. Nastran linear analysis was used in this study because of the large number of variations to the configuration needed to conduct the parametric study. No structural damping was added for this analysis. Figure 16 shows the effect of nacelle weight on the flutter boundary for the nominally stiff pylon, superimposed on the TDT operating envelope. Similarly, Fig. 17 shows the effect of nacelle weight on the flutter boundary for the 75% stiff pylon, superimposed on the TDT operating envelope. It can be seen that the highest engine weight produces the lowest flutter boundary. It can also be seen that for a given nacelle weight the 75% stiff pylons give a lower flutter boundary than the nominally stiff pylon. As a result of the parametric study, two configurations were chosen for the first open-loop test, a nominal configuration using the nominal pylon stiffness and nominal nacelle weight, and a ballasted configuration using the 75% stiff pylon and nacelles with 2.5 times the nominal weight. The flutter boundaries calculated for these two configurations were valuable guidelines for the test engineers during the wind-tunnel tests. The results of the parametric study predicted that the ballasted configuration would go unstable at a lower dynamic pressure than the nominal configuration. These results were confirmed

during the first open-loop test, and only the ballasted configuration was used in the final three wind-tunnel tests and in all further computational analyses.

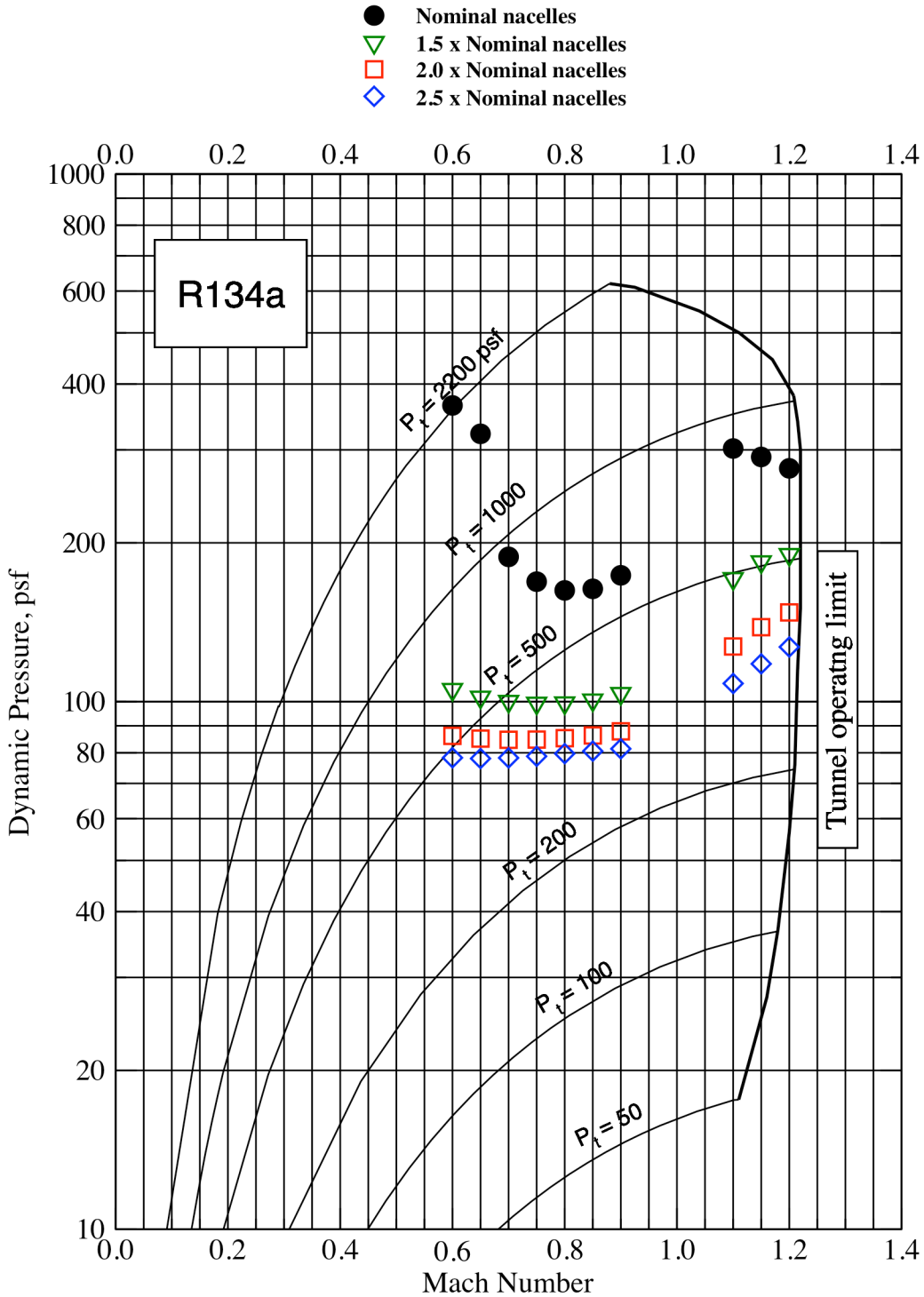


Figure 16. Predicted flutter boundary variation with nacelle weight for the nominally stiff pylon using linear analysis.

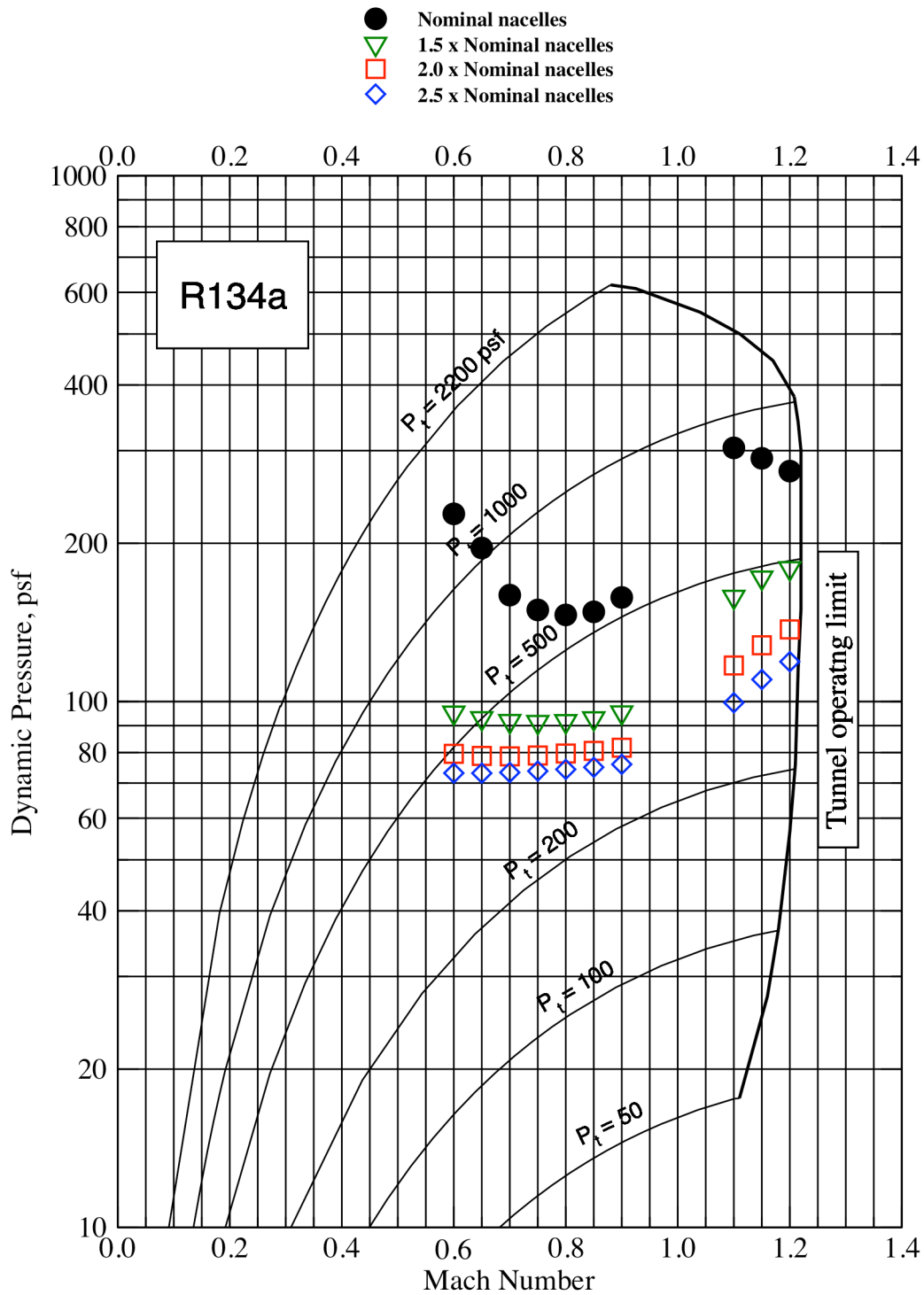


Figure 17. Predicted flutter boundary variation with nacelle weight for the 75% stiff pylon using linear analysis.

A second parametric study was performed later in the test program. As a result of examining the results of the nonlinear flutter analysis, it was discovered that the S⁴T configuration is unusually sensitive to the amount of structural damping assumed to be present in the structure. The best nonlinear results were achieved when the structural damping obtained from GVTs was used. Once this was discovered, a new parametric study was performed to determine the effect of structural damping on the linear flutter boundary. Figure 18 shows the effect on the flutter boundary of using a constant value of structural damping in each flexible mode and using GVT-based damping, compared to the experimental flutter results. Unfortunately, for safety reasons the experimental flutter dynamic pressure could not be reached for supersonic flow, although it is known to be above 101.06 psf, which is the highest dynamic pressure reached during the wind-tunnel tests. The details of how the experimental flutter results were obtained can be found in another paper submitted as part of the S⁴T special session⁴. Several conclusions can be drawn from this study. First, it can be seen that the predicted flutter boundary using GVT-based damping is slightly higher than the boundary obtained using a constant value of 2% per flexible mode, but is very conservative compared to the experimental results. Second, in order to match the experimental flutter boundary using linear analysis, an unrealistically high value of structural damping of 6% was required.

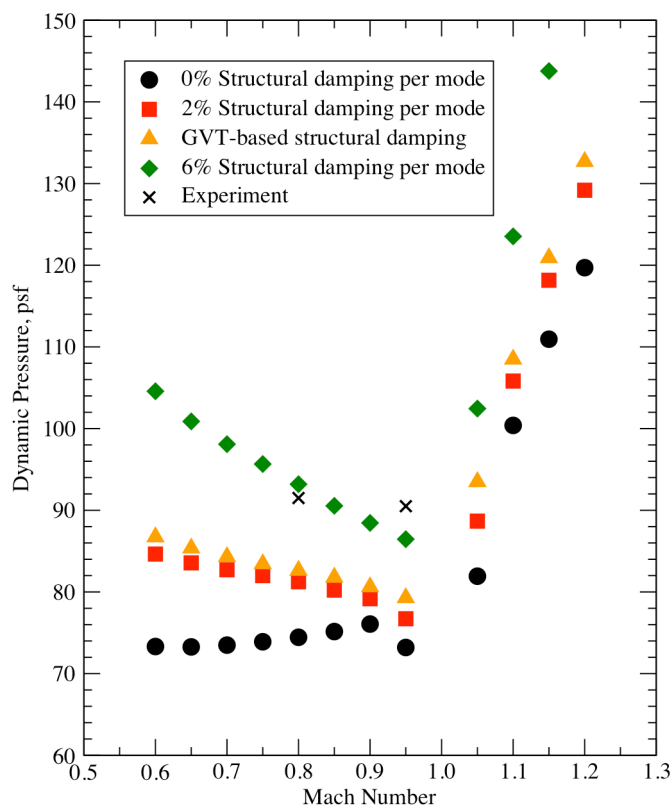


Figure 18. The effect of structural damping on the predicted flutter boundary using linear analysis for the 75% stiff pylon and 2.5 x nominal nacelle weight configuration.

Another useful feature of Nastran's linear analysis is the ability to gain insight into the details of the flutter mechanism. Figure 19 shows the stability plot for a Mach number of 0.80. The bottom plot shows the damping factor, zeta, as a function of dynamic pressure for each of the first five flexible modes. A negative value for zeta indicates a stable system; it can be seen from the bottom plot that the second mode goes unstable at a dynamic pressure of 82 psf. The top plot tracks the frequency of each of the first five flexible modes as a function of dynamic pressure. It can be seen from this plot that the flutter mechanism is a coalescence of the first two flexible modes. Figures 20 and 21 show the stability plots for Mach numbers of 0.95 and 1.10 respectively. In these cases it is the first flexible mode that goes unstable, but the flutter mechanism is consistent as a coalescence of the first two modes.

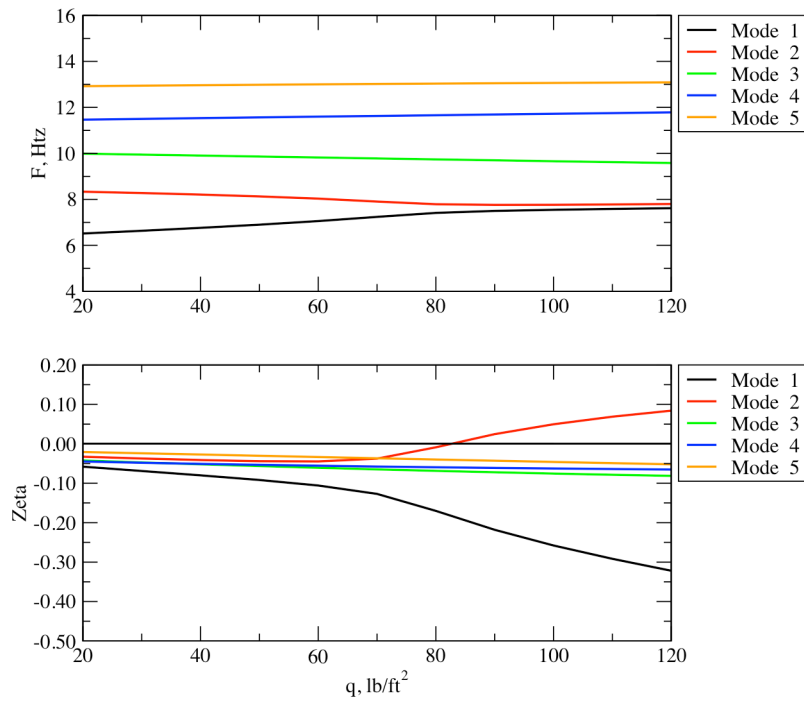


Figure 19. Stability plot for linear analysis at Mach = 0.80.

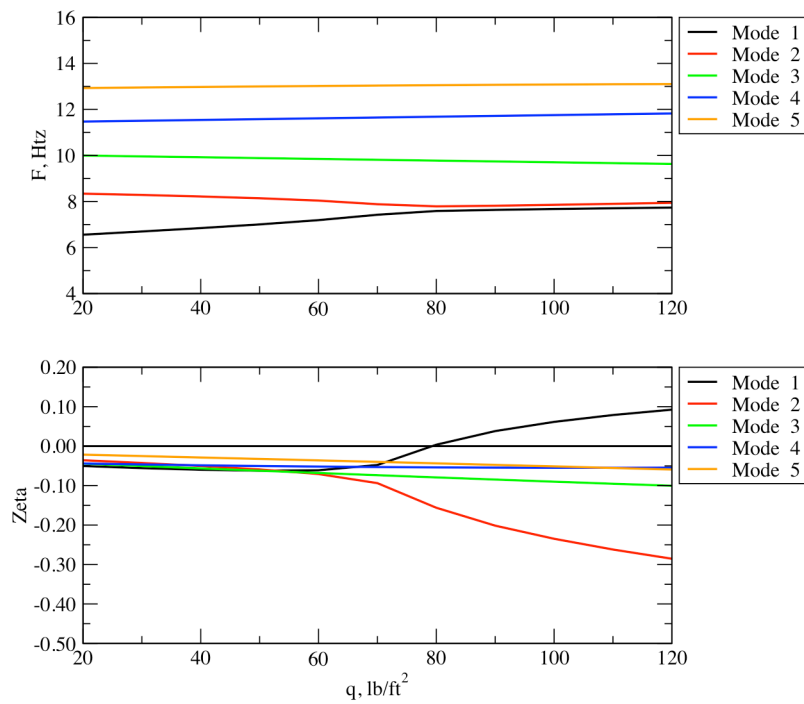


Figure 20. Stability plot for linear analysis at Mach = 0.95.

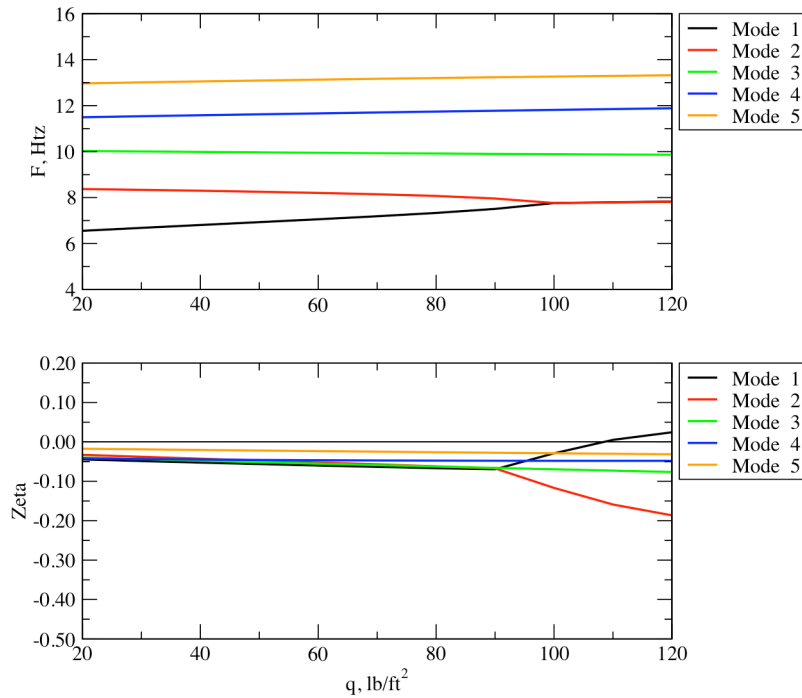


Figure 21. Stability plot for linear analysis at Mach = 1.10.

IV. Nonlinear Aeroelastic Analysis

While the linear analysis available in Nastran gives quick results, it breaks down in the transonic flight regime. A more sophisticated analysis, such as the Computational Aeroelastic (CAE) capability found in the CFD code CFL3D Version 6.4, is needed for the analysis in this speed range. The full nonlinear analysis using CFL3D consists of three steps. First, a steady-rigid calculation at a given Mach number, Reynolds number and angle of attack is done to calculate the steady-state flowfield. Next, a static aeroelastic calculation at a given dynamic pressure is performed to determine the steady-state deflections due to the flexibility of the structure. Since only the final deflected shape and not the time history of the deflections is needed, an unrealistically large amount of structural damping is added to the structure to shorten the amount of computational time needed for the calculations. In the third and final step, the structural damping is returned to an accurate value, and a time-accurate simulation is begun with a pulse in the modal velocity of one of the structural modes. If this disturbance dies out, the given dynamic pressure is below the flutter threshold. If the dynamic pressure is too high, a flutter condition occurs and the disturbance grows uncontrollably. This analysis is repeated, varying the dynamic pressure until a neutrally stable condition is reached. All static and dynamic aeroelastic calculations were performed using the first ten flexible modes.

In addition to providing the first step in the aeroelastic analysis, the steady-rigid calculations were used to assess the quality of computational grids that had been developed for the project, to verify that they had sufficient resolution to capture the physics of the flowfield. Figure 22 shows the surface grid used in the CFD analysis. Figure 23 shows a sample result from the steady-rigid analysis, pressure coefficient contours for inviscid flow at a Mach number of 1.10 and an angle of attack of zero degrees.

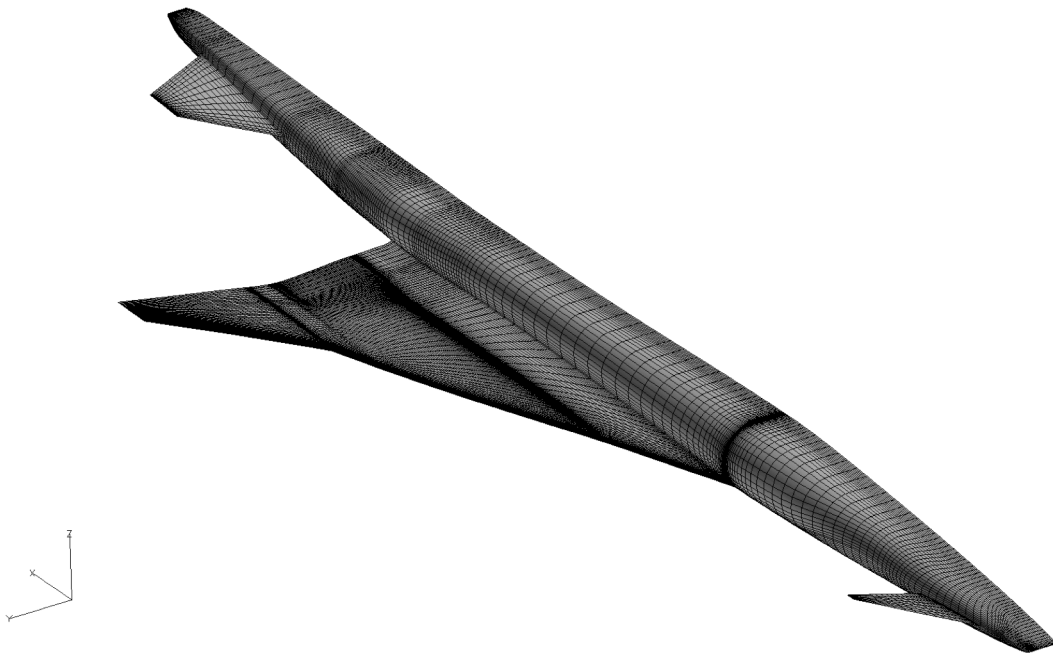


Figure 22. CFD surface grid.

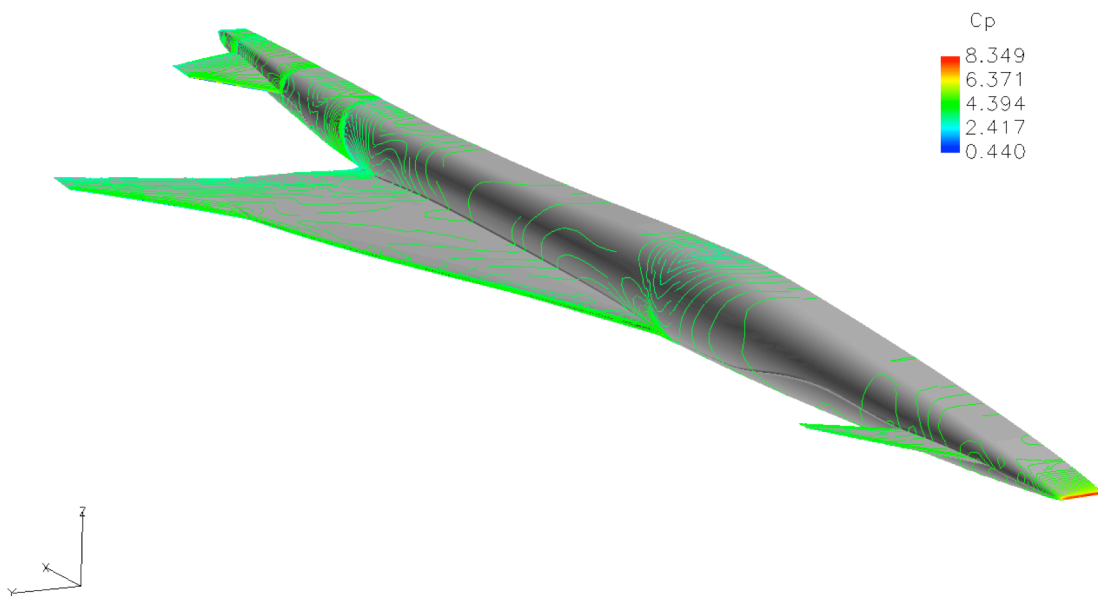


Figure 23. Pressure coefficient contours for inviscid flow at Mach 1.10 and zero degrees angle of attack.

The majority of the computational effort was spent in determining the flutter boundary using the dynamic CAE procedure described above. Both inviscid and viscous calculations were performed. Both the inviscid and viscous grids consisted of 5.4 million grid points and 74 blocks. The only difference between the inviscid and viscous grids was the minimum spacing at the solid surface and the grid stretching rate in the direction normal to the solid surfaces. This was done for convenience, so that the same block connectivity information could be used for both types of grid. The Reynolds number for each case was chosen to agree with the Reynolds number for the corresponding wind-tunnel test conditions, which ranged from 50,000 per inch to 150,000 per inch depending on the Mach number and dynamic pressure. In the finite element model the engine nacelles are modeled as a series of concentrated masses and rigid body elements in a cruciform shape. Because of the difficulty smoothly interpolating the limited number of nodes in the finite element nacelle definition onto the engine nacelles of the computational surface grid, it was decided to remove the engine nacelles from the CFD grids. Steady rigid test cases showed little difference in lift and drag between the nacelle-on and nacelle-off configurations. While the aerodynamic effects of the engine nacelles were omitted from the nonlinear aeroelastic calculations, the inertial effects of the nacelles were taken into account via the mode shapes obtained from the finite element modal analysis.

Figure 24 shows the generalized displacement history of the first flexible mode for inviscid flow at a Mach number of 0.95 for the case of 1% structural damping per flexible mode. It can be seen that the solution is neutrally stable at a dynamic pressure of approximately 45 psf. Figure 25 shows the generalized displacement history of the first flexible mode for viscous flow, where the simulation is close to being stable at a value of 75 psf. The fact that the displacement is very slowly diverging at 75 psf indicates that the flutter dynamic pressure is slightly above this value. This is a typical result, with the flutter dynamic pressure for the inviscid calculation being more conservative than that of the viscous calculation, and much too conservative when compared to the experimental results. Because of this, most of the effort concentrated on viscous flow analysis.

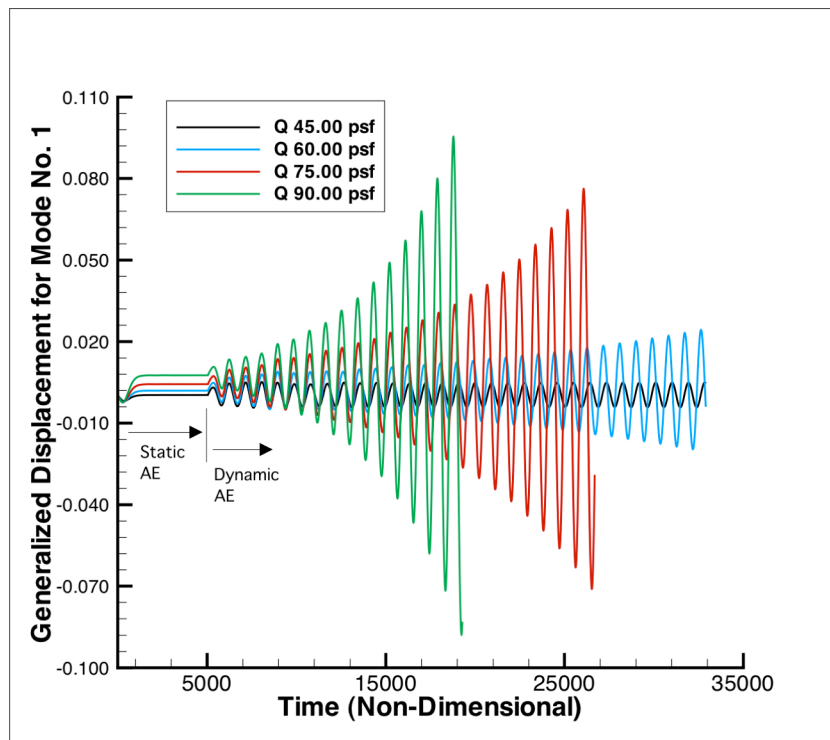


Figure 24. Response of the first mode generalized displacement at Mach 0.95 for inviscid flow.

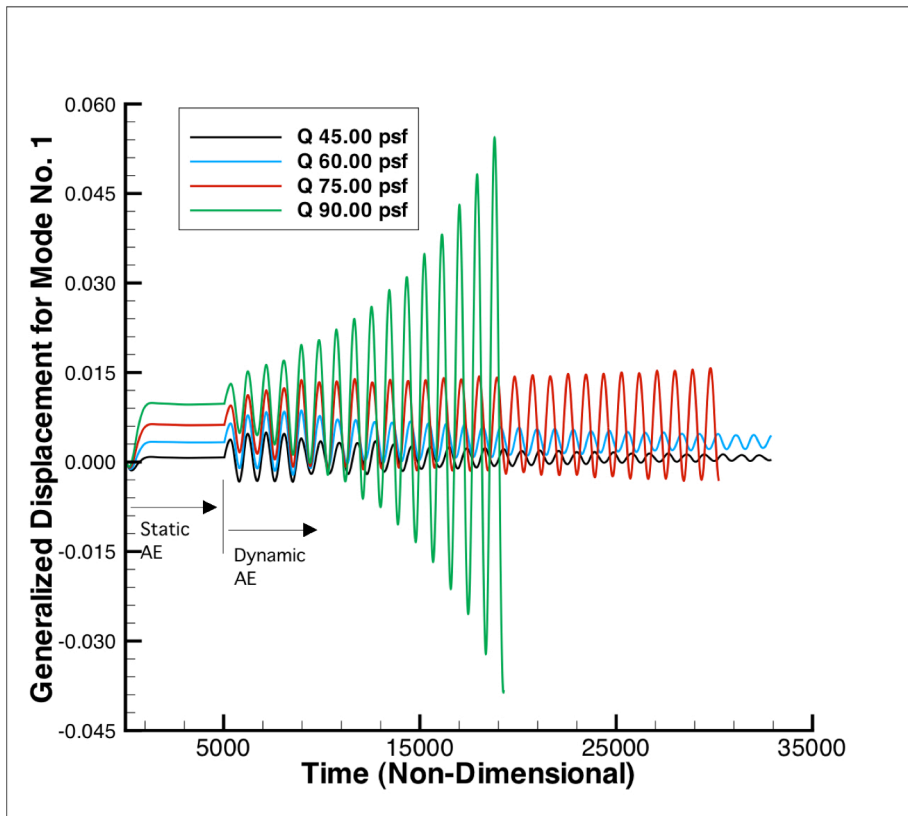


Figure 25. Response of the first mode generalized displacement at Mach 0.95 for viscous flow.

The initial comparisons of the nonlinear flutter boundary with the experimental results did not agree well. The final closed-loop wind-tunnel test in the TDT determined that the flutter dynamic pressure for Mach numbers of 0.80 and 0.95 were in the vicinity of 90 psf. However, the computational results gave flutter dynamic pressures much lower. As mentioned in the previous section, the value of structural damping used in the computations was very important. The initial computational results used a value of structural damping of one percent for each flexible mode, which is typical for studies done in the past. However, when structural damping values obtained from GVTs were used, the flutter dynamic pressure agreed well with the experimental results. Figure 26 shows a comparison of the flutter boundary determined using constant structural damping and GVT-based structural damping, compared to the experimental results.

The results of this analysis emphasize the importance of having an accurate value of the structural damping for the configuration, which is impossible to obtain if there are no GVT results available. The high cost of wind-tunnel testing has resulted in a higher reliance on computational methods for the analysis of N+2 and N+3 configurations. The lack of important information such as accurate values of structural damping will increase the uncertainty of these analyses.

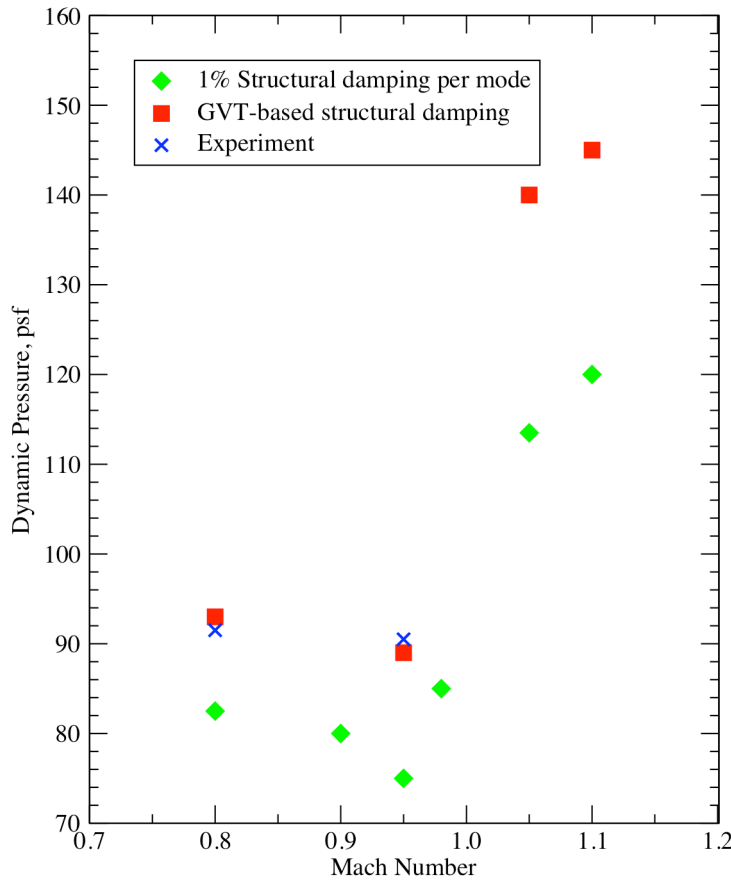


Figure 26. The effect of structural damping on the predicted flutter boundary using nonlinear analysis for the 75% stiff pylon and 2.5 x nominal nacelle weight configuration.

V. Reduced Order Models

Development of aeroelastic reduced-order models (ROMs) was performed using CFL3D viscous solutions^{5,6}. These ROMs can be used within a MATLAB®/Simulink® environment to create root locus plots that exhibit the migration of the aeroelastic roots. Presented in Fig. 27 is a root locus plot at a Mach number of 0.80 indicating the coalescence of the first and second modes leading to flutter at a dynamic pressure of 86.4 psf using GVT-derived structural damping. This result is more conservative than the full CFL3D prediction. Figures 28 and 29 show the root locus plots for Mach numbers of 0.95 and 1.05, respectively. The flutter predictions for these two Mach numbers agree well with the full CFL3D results.

The flutter mechanisms obtained from the root locus plots from the ROM analysis can be compared to the flutter mechanisms obtained from the linear analysis. Overall, the agreement is good. In all cases, the flutter mechanism involves the coalescence of the first two flexible modes. In the linear analysis, the second mode goes unstable in the subsonic case, and the first mode goes unstable in the transonic and supersonic cases. In the ROM analysis, the second mode goes unstable in the subsonic and supersonic cases, while the first mode goes unstable in the transonic case.

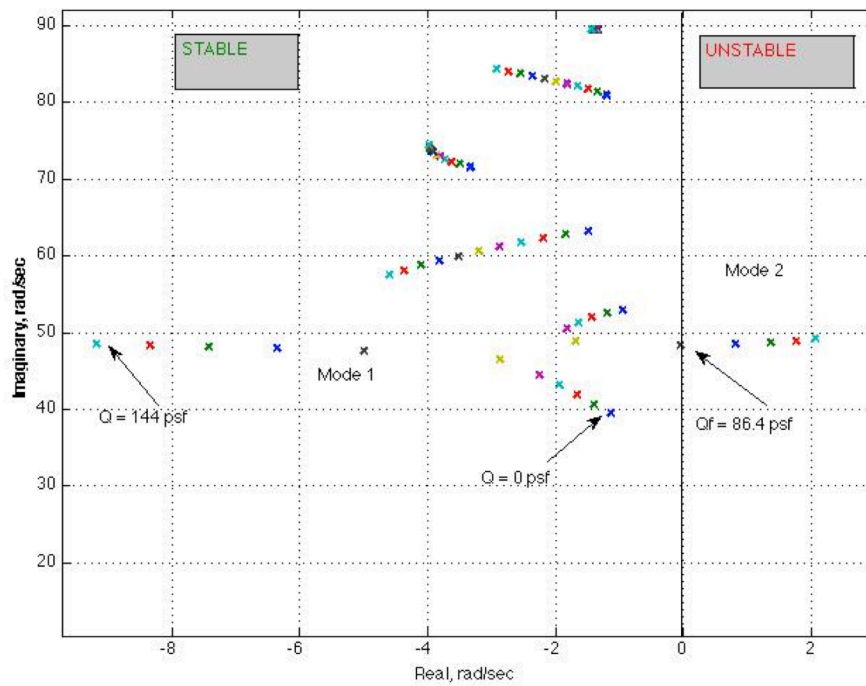


Figure 27. Root locus from ROM for Mach 0.80

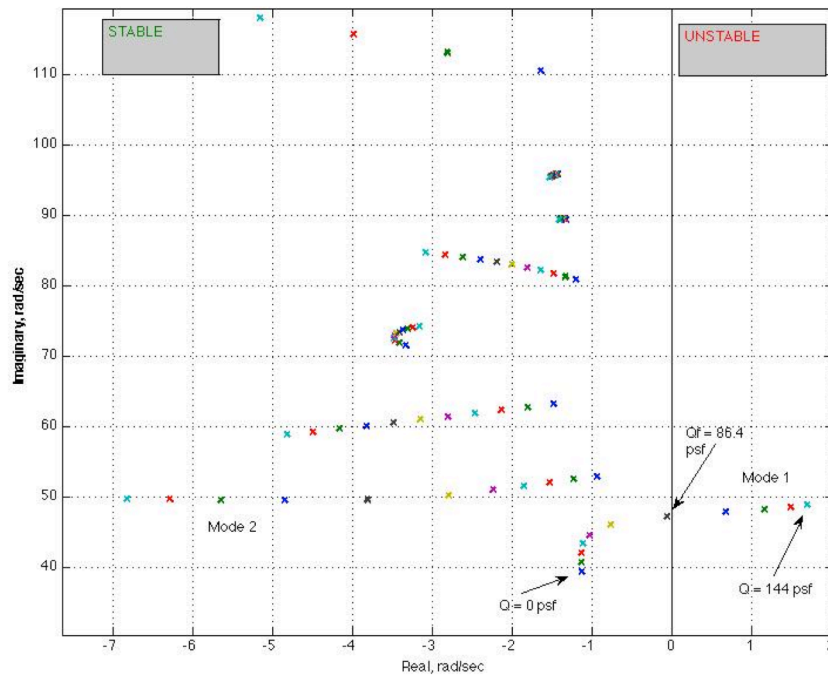


Figure 28. Root locus from ROM for Mach 0.95

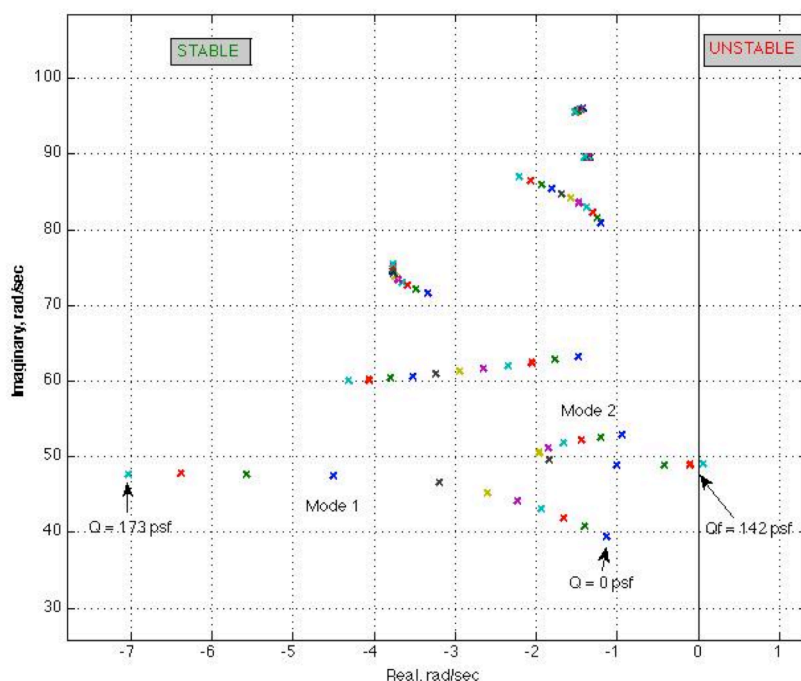
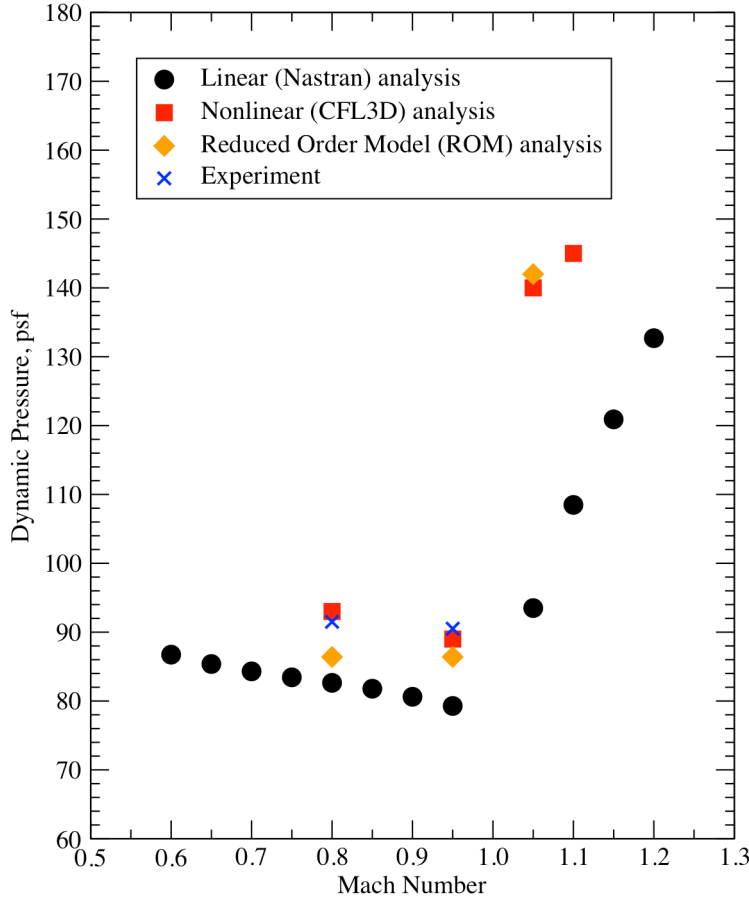


Figure 29. Root locus from ROM for Mach 1.05

VI. Analysis Summary

A variety of computational methods were used in the analysis of the S⁴T wind-tunnel model, including linear methods, nonlinear CFD-based methods and ROM methods. Figure 30 shows the most up-to-date results for each method compared to the experimental results.

Each computational method has its advantages and disadvantages. Linear methods are very cost effective; an entire flutter boundary with 12 different Mach numbers can be calculated in less than 30 minutes of wall clock time on a high end PC or small cluster. However, the linear methods consistently under predicted the flutter dynamic pressure, even in the subsonic range. Thus linear methods are good for parametric studies, such as those that compare different versions of the finite element model, but are not useful for an accurate prediction of where flutter will occur. The nonlinear analysis using CFL3D gives much more accurate results, but is orders of magnitude more expensive to conduct. Unfortunately, finding the flutter boundary using this method is a trial and error process, where multiple dynamic pressures are chosen until a neutrally stable solution is found. The solution for a single dynamic pressure can easily take a day or more using a high-end parallel machine such as those found at NASA's NAS facility; the entire process can easily take on the order of a week to find the flutter point for a single Mach number. Analyses using Reduced Order Methods are relatively new, and provide a potential for obtaining accurate flutter predictions at a greatly reduced cost. ROM-based solutions are comparable in accuracy to solutions using computational aeroelasticity methods. However, for a given Mach number the ROM analysis requires only a single time accurate solution from CFL3D. Once this solution is obtained, a ROM can be generated in a few minutes on a high-end PC or small cluster. After this, a full flutter solution over a large number of dynamic pressures can be generated in a matter of seconds. Because both the nonlinear and ROM analyses use CFL3D, the set up time, including grid generation, validation of the grid, and interpolating the flexible modes onto the CFD grid, is the same. However, once the setup procedure is completed, generating accurate flutter results can be done much more quickly using a ROM-based analysis.



VII. Future Work

The computational analysis of the S⁴T configuration is a work in progress. It is not understood why the linear analysis consistently under predicted the flutter dynamic pressure, especially at low Mach numbers. One possible source of error is the fact that the fuselage surface was modeled as a lifting body in the linear doublet lattice box structure, while on the wind-tunnel model it was a rigid fiberglass shell attached to the backstop. The additional aerodynamic loads from the inclusion of the fuselage surface could lower the predicted flutter boundary. The effect of the fuselage surface on the linear flutter boundary is currently being investigated. Further analysis is also needed to determine why the ROM results for a Mach number of 0.80 agree so poorly with the full CFL3D results. Work is also continuing to calculate the flutter point for additional Mach numbers using both the full CFL3D analysis and ROMs. Filling in the flutter boundary will help to better understand the flutter characteristics of the S⁴T configuration, especially in the transonic regime. The effect of angle of attack on the flutter results can also be investigated. Although there was insufficient time during the wind-tunnel tests to conduct a detailed study of the effects of angle of attack, such an investigation could easily be done computationally.

A new tool has recently been added that will allow the analysis to be taken in new directions. CFL3D has recently been modified to allow full aeroservoelastic simulations⁷. Analysis on the S⁴T to date has concentrated on open-loop (control law off) flutter simulations. The new code, called CFL3D-ASE, incorporates a control law into the system to allow closed-loop (control law on) simulations. In this way, control laws that were tested in the wind-tunnel can be simulated numerically. Once this capability has been validated, it will be possible to perform simulations at conditions that would be unsafe to conduct in the wind-tunnel. In addition, control laws designed for ride quality improvement and gust load alleviation can be simulated and compared to experimental results. Validating this new capability using a complex configuration such as the S⁴T will add a valuable tool for the future analysis of N+2 and N+3 configurations.

REFERENCES

- ¹Silva, W.A., Perry, B., Florance, J. R., Sanetrik, M. D., Wiesman, C. D., Stevens, W. L., Funk, C. J., Hur, J., Christhilf, D. M., and Coulson, D. A., “An overview of the Semi-Span Super-Sonic Transport (S⁴T) Wind-Tunnel Program”, 53rd Structures, Structural Dynamics, and Materials Conference, AIAA, Honolulu, HI (to be published).
- ²Florance, J.R., Scott, R. C., Keller, D.F, Sanetrik, M.D., Silva, W. A., and Perry, B., “Design and Characterization Testing of the Semi-Span Super-Sonic Transport (S⁴T) Wind-Tunnel Model”, 53rd Structures, Structural Dynamics, and Materials Conference, AIAA, Honolulu, HI (to be published).
- ³Bartels, R. E., Rumsey, C. L. and Biedron, R. T., “CFL3D Version 6.4: General Usage and Aeroelastic Analysis”, NASA TM 2006 214301, April 2006.
- ⁴Wieseman, C. D., and Christhilf, D. M., “Analytical and Experimental Evaluation of Digital Control Systems for the Semi-Span Super-Sonic Transport (S⁴T) Model”, 53rd Structures, Structural Dynamics, and Materials Conference, AIAA, Honolulu, HI (to be published).
- ⁵Silva, W.A., “Simultaneous Excitation of Multiple-Input/Multiple-Output CDF-Based Unsteady Aerodynamic Systems”, *Journal of Aircraft*, Vol. 45, No. 4, July-August 2008, pp. 1267-1274.
- ⁶Silva, W. A., “Recent Enhancements to the Development of CFD-Based Aeroelastic Reduced Order Models”, 48th AIAA/ASME/ASCE/AHS/ASC Structures, Structural Dynamics, and Materials Conference, AIAA Paper No. 2007-2051, Honolulu, HI, April 23-25 2007.
- ⁷Roughen, K. M., “NASA S4T – Simultaneous Flutter Suppression, Gust Load Alleviation, and Ride Quality Assurance for Supersonic Aircraft at Transonic Conditions – Final Report”, NASA Contract NNL07AA42C, M4 Engineering, Inc., January 2011.